Ligand Binding to Heme Proteins: II. Transitions in the Heme Pocket of Myoglobin

Judith R. Mourant,* David P. Braunstein,‡ Kelvin Chu, Hans Frauenfelder,§ G. Ulrich Nienhaus, Pál Ormos,¶ and Robert D. Young‖

Department of Physics, University of Illinois at Urbana-Champaign, Urbana, Illinois 61801-3080 USA

ABSTRACT Phenomena occurring in the heme pocket after photolysis of carbonmonoxymyoglobin (MbCO) below about 100 K are investigated using temperature-derivative spectroscopy of the infrared absorption bands of CO. MbCO exists in three conformations (*A* substates) that are distinguished by the stretch bands of the bound CO. We establish connections among the *A* substates and the substates of the photoproduct (*B* substates) using Fourier-transform infrared spectroscopy together with kinetic experiments on MbCO solution samples at different pH and on orthorhombic crystals. There is no one-to-one mapping between the *A* and *B* substates; in some cases, more than one *B* substate corresponds to a particular *A* substate. Rebinding is not simply a reversal of dissociation; transitions between *B* substates occur before rebinding. We measure the nonequilibrium populations of the *B* substates after photolysis below 25 K and determine the kinetics of *B* substate transitions leading to equilibrium. Transitions between *B* substates occur even at 4 K, whereas those between *A* substates have only been observed above about 160 K. The transitions between the *B* substates are nonexponential in time, providing evidence for a distribution of substates. The temperature dependence of the *B* substate transitions implies that they occur mainly by quantum-mechanical tunneling below 10 K. Taken together, the observations suggest that the transitions between the *B* substates within the same *A* substate reflect motions of the CO in the heme pocket and not conformational changes. Geminate rebinding of CO to Mb, monitored in the Soret band, depends on pH. Observation of geminate rebinding to the *A* substates in the infrared indicates that the pH dependence results from a population shift among the substates and not from a change of the rebinding to an individual *A* substate.

INTRODUCTION[1]

Myoglobin is a globular protein consisting of 153 amino acids and a heme (Fe-protoporphyrin IX) as the prosthetic group. Textbooks state that the function of Mb is the reversible binding of small ligands such as dioxygen (O_2) and carbon monoxide (CO) at the heme iron (Stryer, 1988). One could expect such a binding process to be simple. It was indeed originally described as a one-step process (Antonini and Brunori, 1971). Flash photolysis experiments performed over wide ranges in time and temperature imply, however, that the binding process is far from simple (Austin et al., 1975). Four phenomena, in particular, produce complexity: 1. multiple wells along the reaction coordinate, 2. conformational substates, 3. protein relaxation after photodissociation, and 4. thermal fluctuations. In the following, we briefly describe how these phenomena affect the ligand binding to myoglobin.

Multiple wells along the reaction coordinate

In the simplest model, CO in the solvent binds to the heme iron in one step. Flash photolysis data, however, show evidence for multiple processes. A model that describes the salient features of the kinetic data uses three wells (states) along the reaction coordinate,

$$A \rightleftarrows B \rightleftarrows S. \qquad (1)$$

Here *A* denotes the state with the CO bound at the heme iron, *B* the state with CO in the heme pocket, and *S* the state with CO in the solvent. At temperatures above about 160 K, all states play a role in the binding process that takes place after photodissociation. Below about 160 K, however, rebinding after photodissociation is geminate and can be described by using only the states *A* and *B*. In equilibrium, all proteins are in state *A*. Immediately after photodissociation, all proteins are in state *B*, and equilibrium is re-established by transitions $B \rightarrow A$. The rate coefficient of these transitions is assumed to be given by the transition state (Arrhenius) relation (Dlott et al., 1983),

$$k(H_{BA}, T) = A_{BA}(T/T_o)\exp(-H_{BA}/RT). \qquad (2)$$

T_o is a reference temperature, taken to be 100 K. We have studied the transition $B \rightarrow A$ in great detail with flash photolysis experiments below about 160 K. One crucial fact emerges unambiguously from these investigations: Rebind-

Received for publication 9 April 1993 and in final form 24 June 1993.

Address reprint requests to G. U. Nienhaus at Department of Physics, University of Illinois at Urbana-Champaign, 1110 West Green Street, Urbana, IL 61801-3080.

*Present address: MS E535, CLS-5, Los Alamos National Laboratory, Los Alamos, NM 87545.

‡Present address: Department of Biochemistry, B476 Beckman Center, Stanford University, Stanford, CA 94305.

§Present address: MS M715, P-6, Los Alamos National Laboratory, Los Alamos, NM 87545.

¶Present address: Biophysics Institute, Hungarian Academy of Sciences, 6701 Szeged, Hungary.

‖Present address: Department of Physics, Illinois State University, Normal, Illinois 61761.

[1]We have already published a number of papers dealing with ligand binding to heme proteins. Here we continue the series and denote an earlier comprehensive paper (Steinbach et al., 1991) as I.

0006-3495/93/10/1496/12 $2.00

ing is nonexponential in time. To describe this fact, we assume that binding is governed by a barrier of height H_{BA} and that different Mb molecules have different barrier heights. The probability of finding a protein with barrier height between H_{BA} and $H_{BA} + dH_{BA}$ is given by $g(H_{BA})dH_{BA}$. The survival probability $N(t)$, i. e., the fraction of proteins still in state B at time t after photodissociation, is then given by (Austin et al., 1975)

$$N(t) = \int g(H_{BA}) \exp[-k(H_{BA}, T)t]\, dH_{BA}. \qquad (3)$$

Eqs. 2 and 3 together describe rebinding between 60 and 160 K well. Below about 60 K quantum-mechanical tunneling is important and Eq. 2 is no longer valid.

Conformational substates (CS)

Three fundamentally different phenomena can produce nonexponential rebinding: multiple pathways for rebinding within each molecule, a protein relaxation occurring on the same timescale as rebinding (Petrich et al., 1991), or conformational substates. Multiple pathways are ruled out by multiple flash experiments (Austin et al., 1975; Frauenfelder, 1978; Frauenfelder, 1983). There is no evidence for a protein relaxation below 160 K that could explain the nonexponential rebinding observed as low as 4 K. The simplest explanation is the existence of substates. Conformational substates occur because a protein with a given primary sequence can fold into a large number of slightly different structures corresponding to energy valleys in a multidimensional conformational energy surface (Austin et al., 1975; Frauenfelder et al., 1979; Frauenfelder et al., 1991). CS were introduced to explain the observed nonexponential time dependence of ligand binding below about 200 K (Austin et al., 1975), but the concept is now supported by many other experiments (Frauenfelder et al., 1988).

The conformational substates in MbCO are arranged in a hierarchy of at least three tiers (Ansari et al., 1985; Ansari et al., 1987). We call the substates of the highest tier CS0, the substates of the next tier CS1, and so on. The Gibbs free energy barriers between the CS are largest in tier 0 and smaller in the lower tiers. Experimentally, an unambiguous separation of the various tiers is not always possible. One approach is to study transitions among CS as a function of temperature. As the temperature is lowered, transitions among the CS0 cease first. A schematic cross section through the energy landscape, showing only CS0 and CS1, is given in Fig. 1. CO bound to the heme iron (state A) shows at least three different stretch bands (McCoy and Caughey, 1971; Makinen et al., 1979; Caughey et al., 1981; Alben et al., 1982, Ansari et al., 1987) characterizing three CS0, denoted by A_0, A_1, and A_3. Evidence for the substates CS1 comes from rebinding as monitored in the individual CO stretch bands (Ansari et al., 1987). The geminate rebinding is different in the three CS0, but it is always nonexponential in time and implies the existence of a large number of CS1 within each CS0.

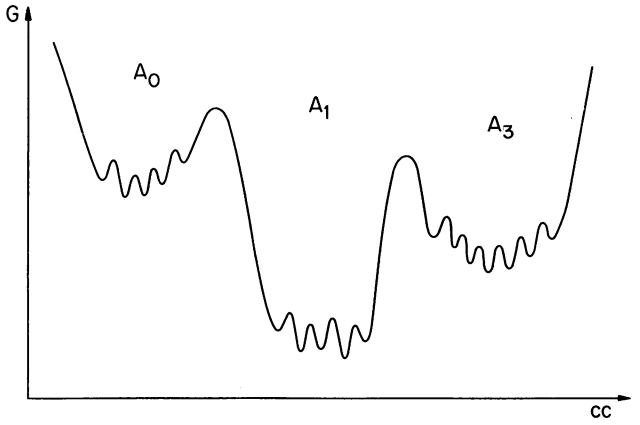

FIGURE 1 Hierarchical arrangement of conformational substates (CS) in MbCO. The diagram represents a one-dimensional cross section through the multidimensional conformational surface. The conformational Gibbs free energy G is plotted as a function of a conformational coordinate *cc*.

Most important for the present work is the top tier of the hierarchy, CS0. The angle, α, between the heme normal and the CO dipole is different in these substates (Ormos et al., 1988; Moore et al., 1988), and we have proposed that the three CS0 have different structures (Hong et al., 1990). Indeed, Phillips and coworkers have found that the distal histidine resides in the heme pocket in A_1, but extends into the solvent in A_0 (Quillin et al., 1992). The structure of A_3 is not yet known. The relative free energies, entropies and volumes of the three CS0 have been determined (Hong et al., 1990). The three CS0 can be described individually, and we therefore call them *taxonomic substates* (Frauenfelder et al., 1991). Their essential properties are summarized in Table 1.

Relaxation phenomena

Equation 3 describes the rebinding well as long as the rebinding barrier in each substate remains constant in time. The structures of Mb and MbCO are, however, not identical. After photodissociation, the protein relaxes toward the Mb structure. The relaxation involves a very rapid elastic shift and a slower conformational change. Agmon and Hopfield (1983) pointed out that this structural change could increase the barrier H_{BA} and slow rebinding. Such a shift in barrier height has indeed been observed (Steinbach et al., 1991; Nienhaus et al., 1992). Fortunately, for the present work, the MbCO structure remains essentially frozen below about 160 K, and we do not have to consider relaxation here.

Thermal fluctuations

At low temperatures, a protein is frozen in a given substate, thus the distribution function $g(H_{BA})$ is time and temperature independent. With increasing temperature, however, more transitions between substates become thermally activated. In other words, the protein begins to fluctuate. Fluctuations can open pathways through the protein and lead to a narrowing and eventual collapse of $g(H_{BA})$ to a δ function at a value $\langle H_{BA} \rangle$.

TABLE 1 Properties of the *A* substates

Substate	Position, ν^* (cm^{-1})			Width, Γ^* (cm^{-1})			$\alpha^‡$	Geminate[§] rebinding
	pH 5.6	pH 6.6	pH 9.0	pH 5.6	pH 6.6	pH 9.0		
A_0	1967.0 ± 0.2	1966.7 ± 0.4		9.6 ± 0.5	9.1 ± 0.5		15°	Fastest
A_1	1947.7 ± 0.2	1946.5 ± 0.2	1945.3 ± 0.2	9.2 ± 0.5	8.1 ± 0.5	9.3 ± 0.5	28°	Interm.
A_3	1934.0 ± 1.0	1933.4 ± 1.0	1928.4 ± 1.0	21.6 ± 1.0	21.8 ± 1.0	19.5 ± 1.0	33°	Slowest

*This work. Band positions and widths were determined from fits of Voigtian line shapes (Ansari et al., 1987) to the measured infrared bands. Temperature: 12 K.

‡From (Ormos et al., 1988), α is the angle between the heme normal and the CO dipole. Temperature: 10 K.

§This work and (Ansari et al., 1987). Temperatures are below 160 K.

The four phenomena described here have been studied in heme proteins, but may be relevant in any protein reaction (Lavalette and Tetreau, 1988; Ehrenstein and Nienhaus, 1992). They make a complete understanding and description of the binding of small ligands at physiological temperatures difficult. At the same time, they are responsible for many or possibly all biologically important aspects of the binding process, and they may also be crucially involved in other biological phenomena. Consider binding of CO to Mb near 300 K. A CO molecule in the solvent will encounter a fluctuating Mb molecule that changes from one taxonomic substate to another. During much of the time, the protein may not have open channels, and the CO cannot enter. During some fluctuations, however, the CO (or even larger molecules like isonitriles) can find an opening and enter the pocket. There it can either bind or exit into the solvent again. During the waiting time in the pocket, the protein may fluctuate to another substate with different binding properties. Once the CO binds, the entire protein changes from the deoxy to the bound-state structure. All of these phenomena can be influenced by temperature, pressure, pH, hydration, solvent and ligand.

In earlier papers we have attempted to separate and characterize these four phenomena (Austin et al., 1975; Alben et al., 1982; Dlott et al., 1983; Ansari et al., 1985; Ansari et al., 1987; Ormos et al., 1988; Hong et al., 1990; Steinbach et al., 1991; Nienhaus et al., 1992). Here we continue the exploration by focusing on phenomena that occur in the heme pocket below about 100 K. We study correspondences between conformational substates of state *B* and state *A*, the time and temperature dependence of transitions between *B* substates, and the effect of pH on the rebinding rate of a given taxonomic substate.

EXPERIMENTAL PROCEDURES

The low-temperature experiments described in the present paper are based on the observation of the CO stretch frequencies both in the bound (*A*) and the photodissociated (*B*) state. In both states, a number of different CO stretch bands are present. We interpret these as indicating different *A* and *B* substates. The *A* substates have stretch frequencies in the range 1910 to 1980 cm^{-1}, the *B* substates extend from about 2110 to 2160 cm^{-1}. Because these ranges do not overlap, motions of the CO in the heme pocket can be followed by monitoring the stretch bands as a function of time and temperature. Two different types of motions can occur after photodissociation, rebinding ($B \rightarrow A$) and transitions between different *B* substates ($B \rightarrow B'$). Rebinding is proven by showing that the decrease in the population of a particular *B* substate is reflected in an increase in the population of the related *A* substate. Transitions between two *B* substates are proven by showing that the disappearance of one matches the appearance of the other, while no changes occur in the *A* bands. We have shown earlier that no transitions between A substates occur below about 160 K (Ansari et al., 1987), and we therefore do not have to consider such transitions here.

In many spectroscopic experiments, the absorbance $\mathscr{A}(\nu, T)$ is measured and interpreted. Here we used Fourier infrared difference spectroscopy (Alben et al., 1982). The MbCO sample was cooled to a temperature of 12 K, where the CO rebinds very slowly. There, a transmission spectrum, $I_d(\nu, T)$, of MbCO was measured. A second transmission spectrum, $I_l(\nu, T)$, was obtained after complete photodissociation of the sample (the subscripts "d" and "l" refer to "dark" and "light"). The absorbance difference spectrum is given by

$$\mathscr{A}(\nu, T) = -\log[I_l(\nu, T)/I_d(\nu, T)]. \quad (4)$$

The difference spectra in Fig. 2 display the *A* substates as negative and the *B* substates as positive absorption bands. The *A* substate with wavenumber closest to that of free CO is denoted by A_0. Evidence for a possible A_2 is inconclusive; we do not consider it here. The notation for the *B* substates differs from our earlier one: we use the low-temperature band position as label.

The difference spectra at a given temperature are insufficient to unravel the connections among the *A* and *B* substates, because the IR bands overlap. We therefore use the idea sketched above: As CO rebinds, *B* bands decrease and *A* bands increase. Related bands must have the same temperature dependence. In principle we could photolyze at a given temperature, take successive spectra to monitor rebinding in the *A* and *B* bands, and repeat the procedure at many temperatures. In practice, it is more efficient to use *temperature-derivative spectroscopy* (TDS) to obtain the kinetic information. TDS is treated in detail in Berendzen and Braunstein (1990). Here we sketch only the basic idea specialized to the present situation. We completely photodissociated MbCO at $T_i = 12$ K, where rebinding is slow. We then

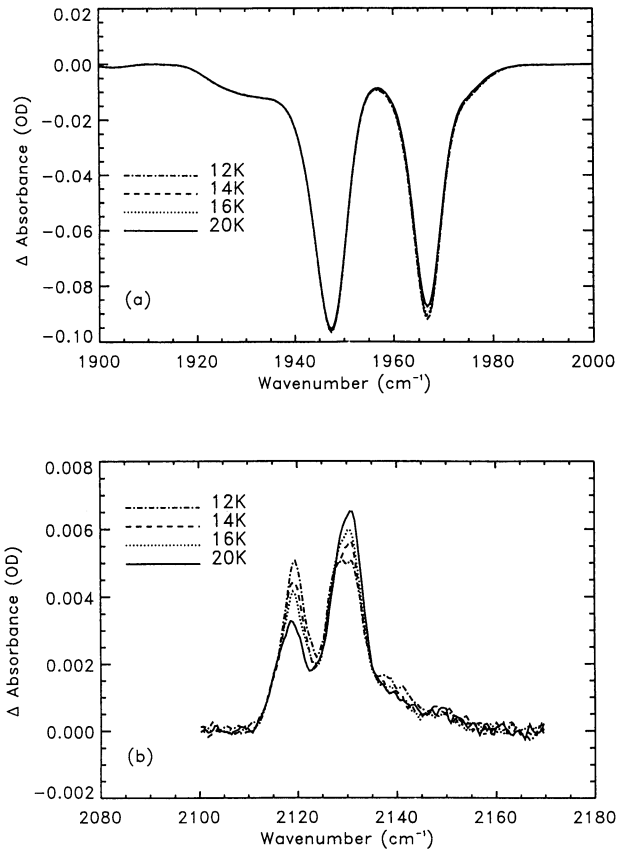

FIGURE 2 Light/dark absorption difference spectra of sperm whale myoglobin in 75% glycerol/buffer, pH 6.0, at temperatures of 12, 14, 16, and 20 K. (*a*) *A* substates; (*b*) *B* substates.

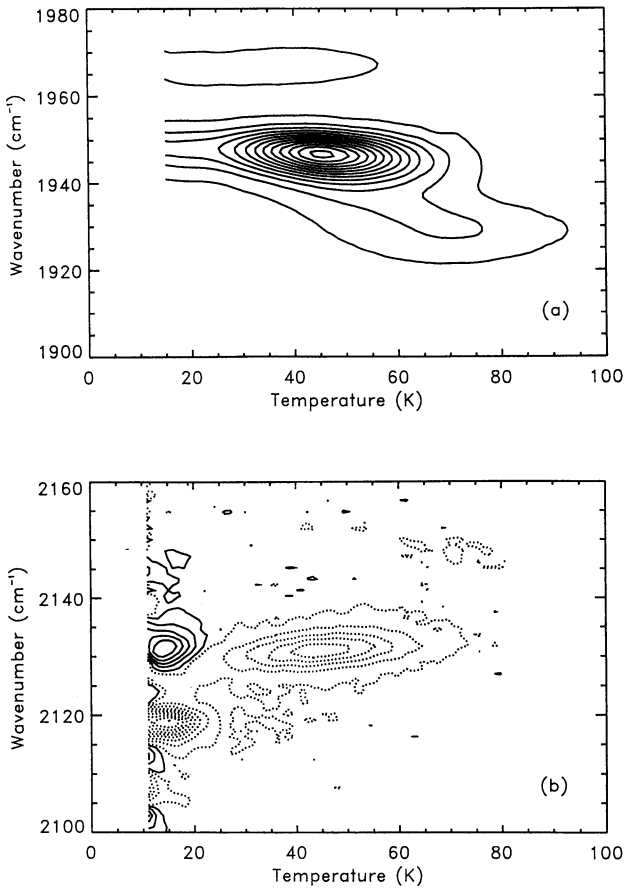

FIGURE 3 TDS contour plots for sperm whale myoglobin sample in 75% glycerol/buffer, pH 6.6. (*a*) Contours of *d*(Absorbance)/*dT* for the *A* substates, spaced at 2 mOD/K. (*b*) Contours of *d*(Absorbance)/*dT* for the *B* substates, spaced at 1 mOD/K. Solid lines are positive contours, and dashed lines are negative contours.

heated the sample in the dark such that $T = T_i + bt$, with $b = 3.125$ mK/s. During the temperature ramp, spectra between 1800 and 2300 cm^{-1} were continuously taken, so that 109 spectra were obtained during a TDS run. Successive spectra are separated in temperature by $\Delta T = 1$ K. If the number, $N(\nu)$, of molecules characterized by the stretch frequency ν is proportional to the absorbance $\mathcal{A}$, we find

$$\frac{dN}{dT} \propto \frac{d\mathcal{A}}{dT} \approx \Delta\mathcal{A}(\nu, T + \Delta T/2)$$
$$= \mathcal{A}(\nu, T + \Delta T) - \mathcal{A}(\nu, T)$$
$$= -\log[I(\nu, T + \Delta T)/I(\nu, T)]. \quad (5)$$

Changes in the population of a particular substate can be obtained from the changes in the absorbance at the relevant wavenumber with increasing temperature. The values of $\Delta\mathcal{A}(\nu, T)$ are represented as contour lines in the (ν, T) plane. Two examples of such TDS maps are shown in Fig. 3. Note first that the maps do not give absorbances, but differences in absorbances and hence differences in the populations of the various substates. The solid lines correspond to increasing absorbances and hence increasing populations. The dotted lines indicate decreasing absorbances and decreasing populations.

As an example of the information contained in the TDS maps, consider Fig. 3 *a*, which depicts rebinding to the three *A* substates listed in Table 1. The pronounced feature centered at 1945 cm^{-1} reflects rebinding to A_1. The feature at 1966 cm^{-1} represents rebinding to the A_0 substates, the one at 1933 cm^{-1} is due to rebinding to A_3.

As a second example, consider the TDS map of the *B* substate region in Fig. 3 *b*. Two different kinetic processes are seen here, namely exchange between two *B* substates and rebinding. An example for the first process is the pronounced positive feature at 2131 cm^{-1} that is accompanied by a negative feature at 2119 cm^{-1} at temperatures below 20 K. No feature with the same temperature dependence is seen in the *A* substate map, and therefore, the process must be the exchange *B2119* → *B2131*. An example of the second process is represented by the negative feature at 2131 cm^{-1} that has the same temperature dependence as the positive A_1 feature in Fig. 3 *a*, with a maximum at 44 K. It must consequently represent the rebinding *B2131* → A_1.

To compare the temperature dependences quantitatively, it is useful to produce "slices" by integrating the TDS maps over the wavenumber interval belonging to a particular substate. The resulting slice is proportional to dN_i/dT, where N_i is the population of substate i. The interpretation

of slices assumes weak kinetic hole burning and that the substates are spectroscopically separated in the selected wavenumber interval. Examples of such slices are shown in Figs. 7, 9, and 10.

For experiments on myoglobin solutions, freeze-dried sperm whale myoglobin was dissolved in a mixture of glycerol and aqueous buffer (3:1, v:v). Potassium phosphate buffer was used for the pH 6.6 sample, citrate buffer for the pH 6.0 and 5.5 samples, and carbonate buffer for the pH 9.0 sample. The protein solutions were stirred for several hours under CO before being reduced with $Na_2S_2O_4$. Final protein concentrations were in the range 10–20 mM. pH was measured at room temperature with a microelectrode (Microelectrodes, Londonderry, New Hampshire) in the sample.

For the experiments on orthorhombic crystals, metmyoglobin crystals were grown at pH 8 according to the procedure outlined by Kendrew and Parish (1956). Selected crystals were reduced with $Na_2S_2O_4$ in CO-saturated mother liquor under anaerobic conditions. Subsequently, the crystals were kept in 1 atm of CO for several hours.

Samples were held between two CaF_2 windows separated by a doughnut-shaped mylar spacer (25 or 75 μm thick) in a cell made out of oxygen-free high-conductivity copper. Temperatures between 12 and 300 K were obtained with a closed-cycle refrigerator (CTI Cryogenics, model 22 C, Waltham, MA) and a digital temperature controller (Lake Shore Cryotronics, model DRC93C, Westerville, OH). Temperatures below 12 K were obtained with a continuous flow dewar. The sample was photodissociated with an argon ion laser (Omnichrome, model 543, Chino, CA). A quarter-wave plate served as a circular polarizer to avoid preferentially photolyzing MbCO molecules with a specific orientation. The laser beam was split and focused down on both sides of the sample to about 1-mm diameter. Transmission spectra were measured with a Fourier-transform infrared (FTIR) spectrometer (Mattson, model Sirius 100, Madison, WI) in the range 1800–2200 cm^{-1} at a resolution of 1 or 2 cm^{-1}. For each spectrum, 470 mirror scans were performed during 320 s. The absorbance difference spectra were calculated according to Eq. 4. Spectra were typically baseline-corrected with a straight line in the *A* substate region and a third-order polynomial in the *B* substate region. Relative substate populations were determined by fitting the baseline-corrected spectra to Voigtians (a Voigtian is the convolution of a Lorentzian and a Gaussian).

The extinction coefficients of the stretch bands in the *A* and *B* substates differ considerably, as is evident from Fig. 2. Alben et al. (1981) suggest a linear relationship between the extinction coefficient and the frequency of the CO stretch band. From their data it is justified to assume similar coefficients within the *A* substates and *B* substates. As a check, we integrated the areas of the *A* and *B* substates and calculated the ratio of the extinction coefficients, $\epsilon_A/\epsilon_B = 22.0 \pm 0.2$. The ratio is independent of pH. Because the relative populations of both the *A* and *B* substates depend strongly on pH, the independence of the ratio on pH implies that the ratio of extinction coefficients of corresponding *A* and *B* substates, $\epsilon_{Ai}/\epsilon_{Bi}$, is very similar for all i (i = 0, 1, 3).

THE CONNECTIONS AMONG THE *A* AND *B* SUBSTATES

Low temperature spectra and photodissociation

A first look at Figs. 2 and 3 suggests that there are three *A* substates and three *B* substates, that *B2118* rebinds to A_0, *B2131* to A_1, and *B2149* to A_3. Closer inspection reveals a problem: Fits of Voigtians to the *A* and *B* bands yields the area ratios $A_0/B2118 = 44$, $A_1/B2131 = 14$, and $A_3/B2149 = 54$. Since the ratio $\epsilon_{Ai}/\epsilon_{Bi}$ is approximately the same for all i (i = 0, 1, 3), the mapping has to be more complex than suggested above.

Data taken at 1 cm^{-1} resolution indicate that there are more than three *B* bands. Fig. 2 shows a slight dip near 2130 cm^{-1} for a fully photolyzed sample at 12 K with a pH of 6.0. Further evidence for two states at about 2128 and 2131 cm^{-1} comes from spectra of samples at pH 6.0 and 6.6 taken at 30 K. The ratio A_0/A_1 is larger at the lower pH. If there are two closely spaced *B* states near 2130 cm^{-1}, one of which rebinds to A_1 and one of which rebinds to A_0, the peak of the band near 2130 cm^{-1} should shift with changes in pH. Indeed, the band occurs at a higher wavenumber at pH 6.6 than at pH 6.0.

The fact that more *B* bands exist than *A* bands leads to three questions: Into which *B* bands does a given *A* substate photodissociate? Do transitions between *B* substates corresponding to a given *A* substate occur after photodissociation? What are the pathways on rebinding? To answer these questions, we used the pH dependence of the IR spectra and the temperature dependence of CO rebinding after photodissociation. Additional information comes from data taken with an orthorhombic crystal sample, in which the substate A_3 is preferentially populated.

To assign *B* substates to a particular *A* substate, we separate the spectra into contributions of the individual *A* substates with their accompanying *B* substates. The pH dependence permits a separation of the *B* substates that belong to A_0 from those that belong to A_1 or A_3. The population ratio A_0/A_1 depends strongly on pH (Fuchsman and Appleby, 1979; Shimada and Caughey, 1982; Ansari et al., 1987; Morikis et al., 1989); the ratio of A_1/A_3 is difficult to determine (owing to the overlap of the bands), but depends only weakly on pH (Fuchsman and Appleby, 1979; Hong, 1988). To achieve the separation, we assume that the shapes and positions of the stretch bands do not depend on pH and write for the absorbance at a given pH

$$\mathcal{A}(\nu; \mathrm{pH}) = \sum f_i(\mathrm{pH})\, \mathcal{A}_i(\nu), \qquad (6)$$

where f_i(pH) denotes the relative population of the substate i, with $\sum f_i = 1$, and $\mathcal{A}_i(\nu)$ is the spectrum of substate i. The coefficients f_i have been determined by fitting Voigtians to the *A* substate spectra at different pH.

Spectra taken at different pH can be normalized and subtracted to yield spectra corresponding to A_0 and $A_1 + A_3$. Such separated spectra are shown in Fig. 4, *a* and *b*. Fig. 4 *a* shows A_0 very clearly, but also displays a bi-lobe feature centered at about 1945 cm^{-1}. We attribute this feature to a pH-dependent peak shift of A_1 (Ansari et al., 1987). Fig. 4, *c* and *d*, are the results of the corresponding subtraction for

the *B* substates. The data in Fig. 4 permit a partial assignment of the substates reached upon photodissociation: *B* substates at 2118, 2128, and 2138 cm^{-1} can be reached from A_0. The *B* substates shown in Fig. 4 *d*, *B2119*, *B2131*, and *B2149*, are reached upon photodissociation of A_1 and A_3. A separation of the substates corresponding to A_1 and A_3 will be performed below. In Fig. 5 *a* we anticipate these results and show the *B* substates that are reached upon photodissociation from the three *A* substates. The relative populations shown refer to 12 K approximately 150 s after photodissociation.

Temperature-derivative spectroscopy and rebinding

Rebinding does not occur simply by reversal of the photodissociation pathways (Alben et al., 1982). A CO molecule may change its position and/or orientation within the pocket before rebinding. To distinguish rebinding and motions in the pocket, we use *A* and *B* substate TDS maps. To illustrate the concepts, assume that an *A* substate A_x leads to substate B_y upon photodissociation and that B_y goes to B_z before rebinding occurs. Since the *B* substate transition does not involve rebinding, there is no signal in the *A* substate map. Rebinding, however, shows up as identical *T* dependence in the *A* and *B* substate maps, with depletion in the *B* and accretion in the *A* maps. Two methods of analyzing the TDS data are described in the following paragraphs.

In order to evaluate the TDS data we note that Eq. 6 should be valid at each temperature if the kinetics of the individual *A* substates is independent of pH and the shapes and positions of the stretch bands do not depend on pH. We therefore generalize Eq. 6 and write,

$$\Delta\mathcal{A}(\nu, T; \mathrm{pH}) = \sum f_i(\mathrm{pH})\, \Delta\mathcal{A}_i(\nu, T). \qquad (7)$$

If TDS data are taken at several different pH values with markedly different *A* substate populations, Eq. 7 can be inverted to give $\Delta\mathcal{A}_i(\nu, T)$ maps that correspond to rebinding to the individual *A* substates. TDS maps corresponding to the substates $A_1 + A_3$ and A_0 are shown in Fig. 6, *a* and *b*. The *B* substate regions from the same data are shown in Fig. 6, *c* and *d*, respectively. These maps are gold mines of information concerning transitions within the heme pocket. We first notice that the TDS map corresponding to A_0 shows a bi-lobe feature near 1946 cm^{-1}, extending from about 20 to 60 K. One lobe corresponds to the disappearance, the other to the appearance of an absorption signal. This behavior is explained by a shift in the peak position of A_1 from about 1947 to 1946 cm^{-1} in going from low to high pH, as shown in Fig. 8 of Ansari et al. (1987). The assumption underlying Eqs. 6 and 7 that the shapes and peak positions of the stretch bands is independent of pH is not rigorously satisfied. A_1 cannot be completely subtracted out of the A_0 spectrum. However, the pH dependence of the peak position of A_1 detracts only slightly from the usefulness of the maps for connecting the *A* and *B* substates.

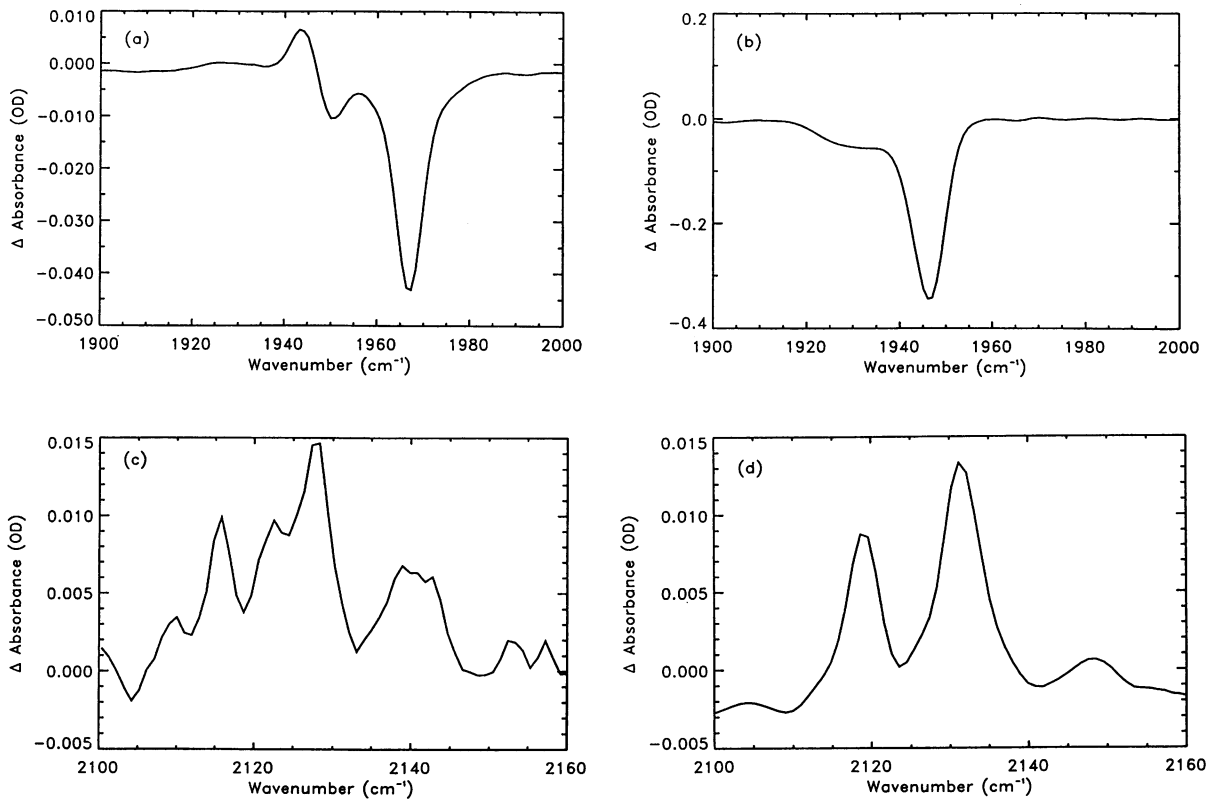

FIGURE 4 Subtractions of light/dark absorbance difference spectra taken with MbCO samples at different pH to isolate the spectra of (*a*) A_0 (pH 6.6–6.0), (*b*) $A_1 + A_3$ (pH 6.0–9.0), (*c*) *B* substates connected to A_0, and (*d*) *B* substates connected to $A_1 + A_3$.

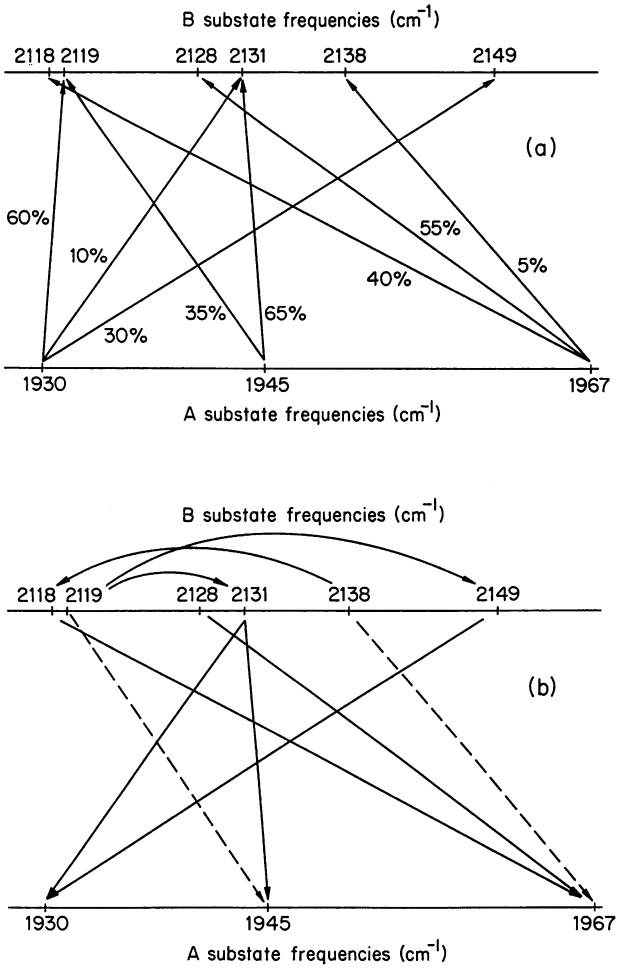

FIGURE 5 (*a*) *B* substates reached by photodissociation from the *A* substates. (*b*) Rebinding pathways from the *B* substates. The dashed lines indicate that only a small fraction of ligands rebinds via these pathways.

Rebinding to A_0

The TDS map corresponding to A_0 in Fig. 6 *a* and the corresponding *B* state map (Fig. 6 *c*) give information about which *B* substates rebind to A_0. There are several pathways leading to A_0, namely *B2118* $\rightarrow A_0$, *B2128* $\rightarrow A_0$, and *B2138* $\rightarrow$ *B2118* $\rightarrow A_0$. *B2138* may also rebind directly to A_0. These assignments are verified by matching the *B2128*, *B2118*, and A_0 slices in Fig. 7 *a*.

Rebinding to A_1

A comparison of Figs. 6 *b* and 6 *d* provides strong evidence that *B2131* rebinds to A_1. Moreover, the integrated decrease in the *B* map from 2131 to 2134 cm^{-1} and the increase in the *A* map from 1945 to 1950 cm^{-1} have nearly identical temperature dependencies above 30 K as shown in Fig. 7 *b*. This agreement verifies the assignment that *B2131* rebinds to A_1.

Rebinding to A_3

The method employed so far does not permit an unambiguous separation of A_1 and A_3. Two other approaches are possible, however. First we use the temperature dependence of rebinding. Fig. 6, *b* and *d*, shows that the temperature dependencies of the signals from A_3 and *B2149* are similar. To quantify this observation, we produce slices by integrating $\Delta\mathcal{A}(\nu, T)$ over the two substates involved, namely from 1927 to 1933 cm^{-1} for A_3 and 2149 to 2151 cm^{-1} for *B2149*. The slices shown in Fig. 7 *c* reinforce the assignment shown in Fig. 5 *b*.

A second approach to isolate A_3 is based on the observation by Makinen et al. (1979) that MbCO in crystalline form can, under certain conditions, exhibit a very strong A_3 band. Indeed, the TDS spectrum of an orthorhombic MbCO crystal at pH 8, shown in Fig. 8 *a*, is strikingly different from the solvent spectrum given in Fig. 3 *a*. The substate A_0 is essentially missing, and the population of A_1 is only about 10% that of A_3. The *B* state map in Fig. 8 *b* is also different from the corresponding maps in Fig. 3 *b* and shows that A_3 dissociates predominantly into *B2119*. A comparison between the *A* and *B* state maps indicates that rebinding occurs only from *B2131* and *B2149*, but not from *B2119*. There is no population in *B2119* when rebinding to A_3 begins.

TRANSITIONS BETWEEN *B* SUBSTATES

No transitions between the taxonomic substates A_0, A_1, and A_3 occur below about 160 K, either in the bound state or via the photodissociated state (Ansari et al., 1987). The data in Fig. 6, *c* and *d*, however, demonstrate transitions *B2119* $\rightarrow$ *B2131* and *B2138* $\rightarrow$ *B2118* even at 12 K. The lack of transitions in the *A* substates is explained by assuming that the substates A_0, A_1, and A_3 correspond to three different protein structures (Hong et al., 1990). The barriers between these substates, as measured by pressure jump experiments, are high, and no transitions occur at low temperatures (Iben et al., 1989; Frauenfelder et al., 1990). We interpret the different *B* substates belonging to the same *A* substate as corresponding to different positions and/or orientations of the CO within the heme pocket in a given taxonomic substate. We will justify this interpretation below. The transition *B2138* $\rightarrow$ *B2118*, for instance, then would be the motion of the CO from a position with stretch frequency similar to that of free CO (2143 cm^{-1}), to an alternative position with the pocket conformation unchanged.

Transitions between *B* substates observed in TDS can be of two kinds, equilibrium and nonequilibrium (Alben et al., 1982). In equilibrium transitions, the populations of the *B* substates change with temperature as a result of their different Gibbs free energies. In nonequilibrium transitions, photodissociation initially leads to *B* substate populations that are out of equilibrium. With increasing temperature, transitions toward equilibrium occur. The two cases can be distinguished by first increasing and then decreasing the temperature. In equilibrium transitions, the population of the substates is only a function of *T* and not of the thermal history of the sample. In nonequilibrium transitions, lowering *T* no longer affects the ratio. As shown earlier, the second case occurs here (Alben et al., 1982).

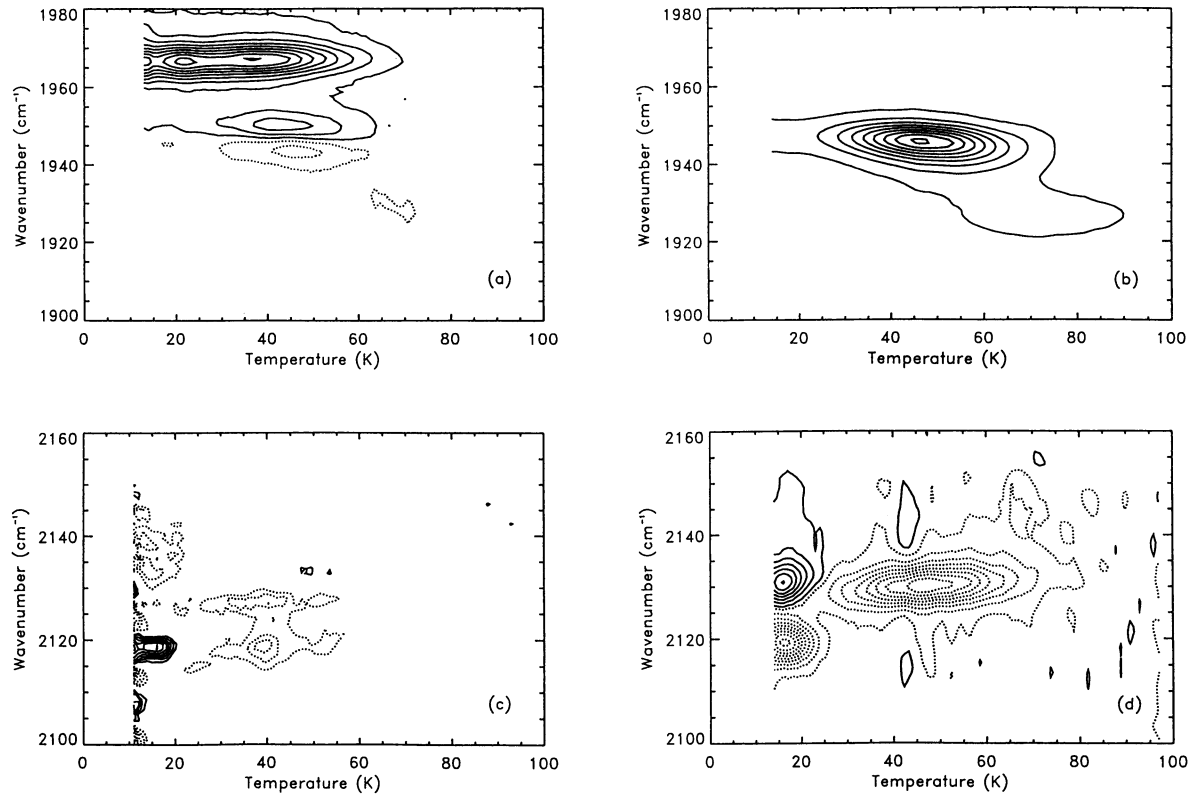

FIGURE 6 Subtractions of TDS maps from MbCO samples at different pH to give contour plots of (*a*) A_0 (pH 6.6–6.0), (*b*) $A_1 + A_3$ (pH 6.0–9.0), (*c*) *B* substates connected to A_0, and (*d*) *B* substates connected to $A_1 + A_3$.

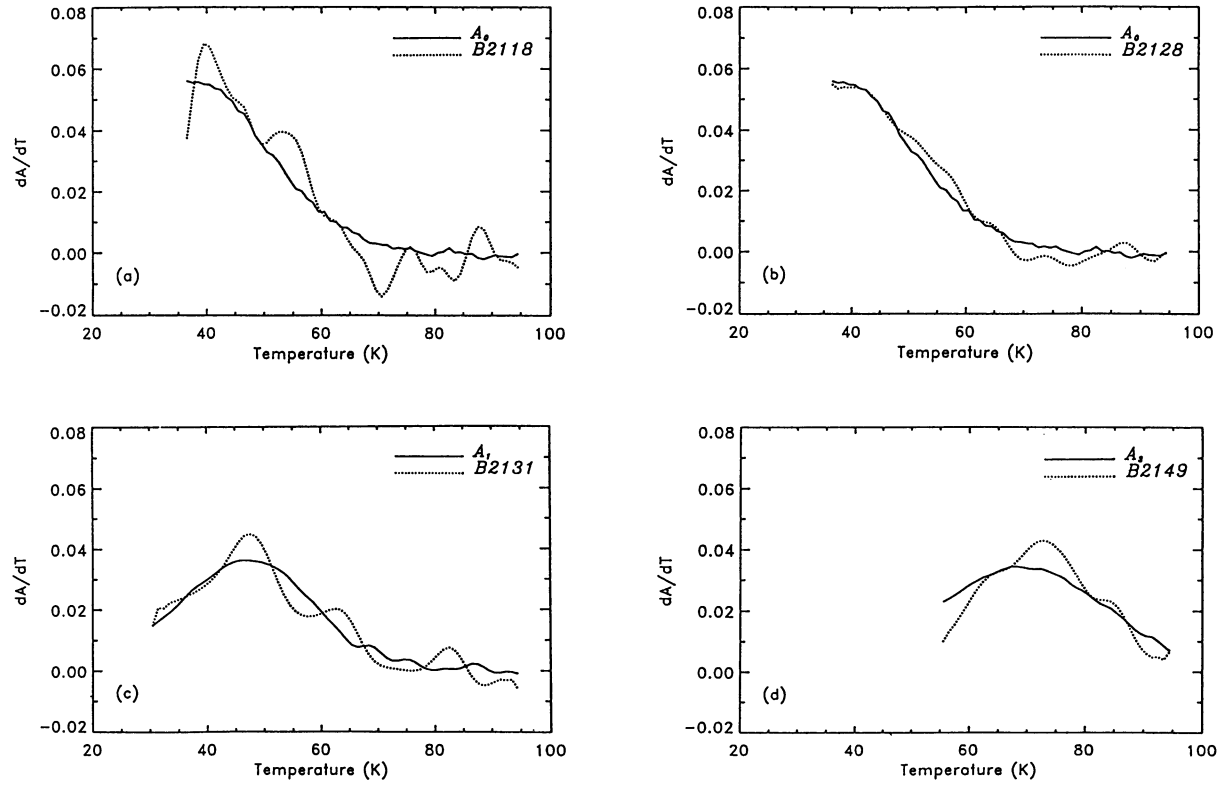

FIGURE 7 Comparison of the rebinding as monitored in the *A* and *B* substates. The TDS signals shown in the maps of Fig. 6 were integrated over a small wavenumber interval to include a particular *A* or *B* substate. The integrated absorbances (slices) of the corresponding *A* and *B* substates were normalized to equal area under the curve. (*a*) Slices for A_0 (1965–1968 cm^{-1}) and *B2118* (2116–2118 cm^{-1}); (*b*) for A_0 (1965–1968 cm^{-1}) and *B2128* (2126–2129 cm^{-1}); (*c*) for A_1 (1945–1950 cm^{-1}) and *B2131* (2131–2134 cm^{-1}); (*d*) for A_3 (1927–1933 cm^{-1}) and *B2149* (2149–2151 cm^{-1}).

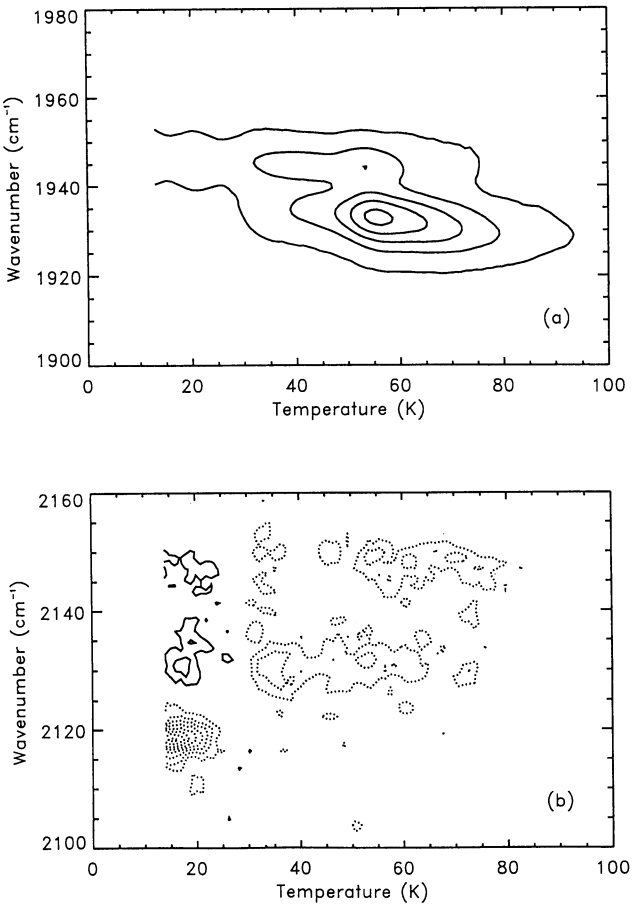

FIGURE 8 TDS contour plots of crystalline MbCO (space group $P2_12_12_1$, pH 8). (*a*) Contours of d(Absorbance)/dT for the *A* substates, spaced at 2 mOD/K. (*b*) Contours of d(Absorbance)/dT for the *B* substates, spaced at 1 mOD/K.

TABLE 2 Properties of the *B* substates

Substate	Position, ν cm^{-1}	Width, Γ cm^{-1}	Rebinds to A_i substate
B2118	2118.4 ± 0.5	7.2 ± 1.0	A_0
B2119	2119.5 ± 0.5	4.5 ± 1.0	A_1 via *B2131*
B2119	2119.9 ± 2.0	10.0 ± 2.0	A_3 via *B2131*and *B2149*
B2128	2127.7 ± 0.5	5.3 ± 1.0	A_0
B2131	2131.1 ± 0.5	5.5 ± 1.0	A_1
B2131	2131.5 ± 2.0	7.3 ± 2.0	A_3
B2138	2138.5 ± 1.0	10.0 ± 1.5	A_0 at least partly via *B2118*
B2149	2149.4 ± 1.5	7.5 ± 1.5	A_3

Band positions and widths determined from fits of Voigtian line shapes (Ansari et al., 1987) to the measured infrared bands. Temperature: 12 K.

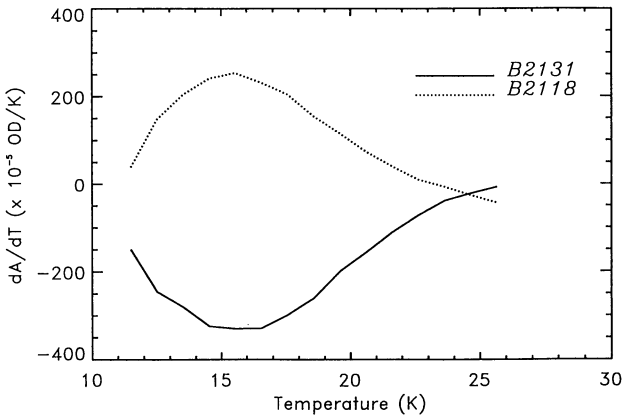

FIGURE 9 Integrated absorbances of B2131 (2130–2133 cm^{-1}) and *B2118*(2117–2121 cm^{-1}) from the TDS map shown in Fig. 6 *d*.

We select the transition *B2119* → *B2131* for a more detailed treatment. The reason for this choice is evident in Fig. 6: Rebinding to A_0 starts at a lower temperature than to A_1. In the transition *B2138* → *B2118*, the competing rebinding to A_0 must be considered, while the transition *B2119* → *B2131* is essentially free of this complication. Fig. 6 *d* shows the transition *B2119* → *B2131* clearly and, together with Fig. 6 *b*, also proves that rebinding to A_1 is negligible below about 25 K.

As a first step in the description of the transitions between the two *B* substates, we look at the overall temperature dependence by integrating $\Delta\mathscr{A}(\nu, T)$ over the intervals indicated in Fig. 6 *d* and fitting the resulting $\Delta\mathscr{A}(T)$ by a third-order polynomial. The result, given in Fig. 9, shows again that the transition in Fig. 6 *d* occurs between the two *B* substates *B2119* and *B2131*.

To determine whether the transition *B2119* → *B2131* is an Arrhenius process or a tunneling process, we measured the spectrum of the *B* states as a function of time after photodissociation at selected temperatures below 25 K. Preliminary data show two features: (i) The survival probability $N(t)$ is nonexponential in time. This observation is in agreement with the broad distribution seen in the TDS maps and verifies the conjecture we made earlier (Alben et al., 1982). (ii) $N(t)$ at 4 and 8 K are identical within error, indicating that the transition occurs by quantum-mechanical tunneling.

PROTEIN ENVIRONMENT AND BARRIER DISTRIBUTIONS

Environmental factors, in particular pH, have large effects on the distribution of rebinding barriers observed in the Soret band (Doster et al., 1982). pH also has a large effect on the relative populations of the *A* substates (Fuchsman and Appleby, 1979; Shimada and Caughey, 1982; Ansari et al., 1987; Morikis et al., 1989). Since the *A* substates rebind with different rate distributions, the question arises if pH affects only the substate populations or if it also changes the rates in different taxonomic substates. To answer the question, we show in Fig. 10 TDS slices for the *A* substates at pH 5.6, 6.0, 6.6, and 9.0. The curves for A_1 in Fig. 10 *b* are all very similar, with the largest deviations occurring at pH 9.0. Similar plots for A_0 and A_3 are shown in Fig. 10, *a* and *c*. Although these plots are noisier, it is still clear that pH has very little effect on rebinding to an individual *A* substate. The change in the overall binding rate with pH is caused by shifts among the taxonomic substates.

While pH does not appear to change the geminate rebinding to each *A* substate, the tight packing of the crystal has a strong effect: The rebinding to A_3 in the glycerol/water sample, Fig. 3 *a*, peaks at 75 K. In the orthorhombic sample, Fig. 8 *a*, the peak occurs at 55 K. Assuming the

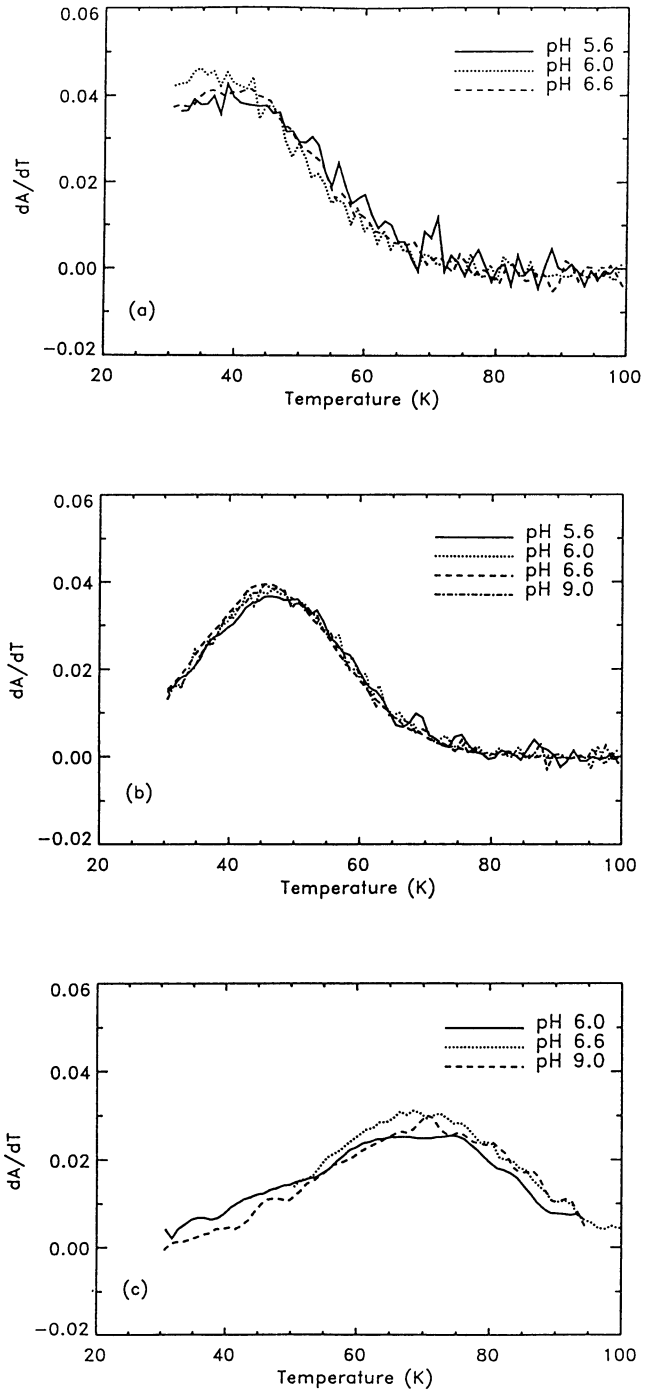

FIGURE 10 Integrated absorbances (slices) for the A substates as a function of temperature. (a) A_0 (1965–1968 cm^{-1}) for pH 5.6, 6.0, and 6.6; (b) A_1 (1945–1950 cm^{-1}) for pH 5.6, 6.0, 6.6, and 9.0; and (c) A_3 (1927–1933 cm^{-1}) for pH 6.0, 6.6, and 9.0.

same preexponential, $A_{BA} = 2.5 \times 10^{10}$ s^{-1} (Young et al., 1991), the shift of 20 K corresponds to a decrease in the peak activation enthalpy by about 5 kJ/mol.

CONCLUSIONS AND OUTLOOK

Even an apparently simple biological reaction, the binding of a small ligand to Mb, is extremely complex and contains parallel and sequential steps. Transitions like those that we have observed at low temperatures will also occur at physiological temperatures and may play an important role in the control of the reactions. The concepts that emerge from the studies of this ligand binding may be of general validity for many other protein reactions. Below, we discuss the main results of the present investigation and raise a number of questions for future studies.

1. The population ratios of the three taxonomic substates (CS0) of sperm whale myoglobin depend on external factors like pH, pressure, and chemical environment. In solution samples, lowering the pH generally leads to a larger fraction in the A_0 substate. We have observed the same behavior with monoclinic MbCO crystals (data not shown), in agreement with recent studies by Champion and collaborators who monitor the A substate populations in the Fe-CO Raman line near 500 cm^{-1} (Zhu et al., 1992). The recent low pH crystal structure of MbCO by Quillin et al. (1992) confirms that the population in A_0 reflects the titration of the imidazole sidechain of the distal histidine (His E7): At high pH, it is neutral and located preferentially in the apolar environment of the heme pocket. As it becomes protonated, it prefers to swing out of the pocket into the polar solvent environment. The $A_0 \rightleftarrows A_1$ transition involves considerable structural changes, which manifest themselves in large activation barriers (Iben et al., 1989; Frauenfelder et al., 1990; Young et al., 1991). While we know how to control the population in A_0, it is not yet clear what determines the amount of A_3. In solution samples, A_3 is only weakly populated, but in the orthorhombic crystal sample, 90% of the population was in the A_3 substate (see Fig. 8). This observation suggests that even a protein as robust as Mb can be strongly influenced by properties of the environment. Makinen et al. (1979) reported that the populations in the various A substates depend on the amount of deoxyMb and metMb in the crystal and speculated that protein-protein interactions between adjacent molecules in the crystal may determine the populations.

2. While the fractional populations of the three taxonomic substates of MbCO in glycerol/water glasses at low temperatures are strongly affected by pH, the rebinding properties within a given CS0 substate remain unchanged. This observation supports our view that the CS0 are three distinct structures of MbCO. The pH dependence of the geminate rebinding, obtained previously from measurements in the Soret region (Doster et al., 1982), can entirely be explained by changes in the CS0 populations. It is interesting that, compared with MbCO in solution, the crystalline sample shows an A_3 substate with significantly modified rebinding properties.

3. Photodissociation from a given A substate can lead to more than one B substate, and the B substates can exchange before rebinding. The connections between the A and B substates are summarized in Fig. 5. Note that there are no connections between the A substates below the glass transition temperature of the solvent. At low temperatures, rebinding always leads back to the same A substate from

which the ligand was photodissociated. Transitions between the *A* substates are only observed above the glass transition of the solvent (Iben et al., 1989; Frauenfelder et al., 1990; Young et al., 1991). In the Introduction, we stressed that the nonexponential geminate rebinding kinetics are caused by structural heterogeneity and not by multiple pathways within a given molecule. However, Fig. 5 shows multiple pathways: *B2118* and *B2128* rebind to A_0, and *B2131* and *B2149* rebind to A_3. Why were they not detected in the multiple flash rebinding experiments? The two *B* substates that rebind to A_0 have virtually the same distribution of rebinding enthalpies, making it impossible to distinguish them in a multiple flash experiment. The two *B* substates that rebind to A_3 have different enthalpy distributions. In principle, they can be detected with a multiple flash experiment. In practice, the effect is difficult to observe in solution samples as the amount of A_3 is rather small. The main conclusions from the original multiple flash experiment (Austin et al., 1975), however, remain unchanged: The nonexponential rebinding arises from conformational substates with different rebinding barriers.

4. The transitions between the *B* substates are nonexponential in time, indicative of distributed conformational barriers between these substates. This observation provides further evidence for the hierarchical arrangement of conformational substates.

The present work establishes a detailed spectroscopic characterization of the *A* and *B* substates. To connect the spectroscopic and kinetic data with structural features, the spatial structures of the individual *A* and *B* substates are needed. X-ray structure analysis will probably be the most powerful tool in these studies. The MbCO structure of Kuriyan et al. (1986) was measured at pH 6 and may contain significant contributions from all three taxonomic substates. To separate the individual *A* substates, one must find conditions under which one of the *A* substates contains the dominant fraction. With this strategy, Phillips and collaborators (Quillin et al., 1992) have recently obtained the x-ray structure of A_0 using a low pH crystal. As we have demonstrated (Fig. 8), there are ways to enhance A_3, but the details are not yet understood. Oldfield and coworkers (1991) developed a molecular model where they explain the *A* substates with four different conformations of the imidazole sidechain of His E7 in the heme pocket, arising from ring-flip isomerization around the C^{β}-C^{γ} bond and $H^{\delta 1}/H^{\epsilon 2}$ tautomerization. The model is based on electrostatic interactions between the imidazole sidechain and the CO molecule. Excellent agreement with the observed stretch frequencies of the heme-bound CO in different heme proteins was reported (Oldfield et al., 1991). Although the A_0 structure that is realized at low pH shows the distal histidine sidechain outside of the pocket, the model by Oldfield et al. still offers a reasonable way to explain the A_1 and A_3 substates.

Structural characterization of the *B* substates is possible by x-ray diffraction of photodissociated MbCO single crystals at cryogenic temperatures. These studies may also be able to elucidate the nature of the transitions between the *B* substates. We interpret the different *B* substates belonging to a particular A substate as representing different locations of the CO in the heme pocket. They could, however, also correspond to different protein conformations. We prefer the former explanation because *B* substate transitions are observed at very low temperatures ($T < 10$ K) and appear to occur by quantum-mechanical tunneling. Tunneling of conformations is less likely because of the larger masses involved. A measurement of the transition *B2119* → *B2131* with different isotopes could help decide this question: Replacement of $^{12}C \rightarrow {}^{13}C$ would affect the CO tunneling rate, but not conformational tunneling. Investigation of the isotope effect for both carbon and oxygen could help distinguish rotational from translational ligand motion. More support for the explanation of the *B* substates in terms of alternate positions of the CO ligand in the pocket comes from the observation that the substates near 2119 and 2131 cm^{-1} occur in all three *A* structures. These lines may arise from similar positions of the CO in the pocket, whereas the location that gives rise to *B2138* may only be accessible in A_0 and *B2149* only in A_3. Recently, Straub and Karplus (1991) performed molecular dynamics simulations and *ab initio* calculations of the CO stretch frequencies in the *B* substates. They pointed out that the interactions between the His E7 sidechain and the CO ligand observed in their simulations should lead to blue shifts with respect to the CO gas phase stretching frequency of 2143 cm^{-1}. Experimentally, only *B2149* shows a blue shift. It was suggested that the red shifts may arise from complexes of the photodissociated CO with phenylalanine sidechains in the heme pocket.

The heme pocket forms an ideal environment for studying the interaction of small ligands with proteins. After the spectroscopic and kinetic characterization, structural information will be necessary to understand the interaction between protein and ligand in detail. To gain more insight into the nature of the *B* substates with spectroscopic methods, experiments with distal pocket mutants will be helpful. Analysis of the spatial structures of these reaction intermediates with structure-resolving techniques (x-ray and neutron scattering, NMR) will also be important for further progress in understanding the connections between spectroscopy, reactivity, and conformation of proteins.

We are grateful to Ilme Schlichting for providing us with orthorhombic metmyoglobin crystals. We thank Yavuz Abadan, Bradley T. Banko, Joel Berendzen, David Ehrenstein, Rick Ernst, Don C. Lamb, Benjamin McMahon, Jochen Müller, Robert Philipp, and Aihua Xie for help and many useful discussions.

This work was partially supported by the National Science Foundation (Grants DMB87–16476 and INT88–10944) and the National Institutes of Health (Grants GM 18051 and 32455).

REFERENCES

Agmon, N., and J. J. Hopfield. 1983. CO binding to heme proteins: a model for barrier height distributions and slow conformational changes. *J. Chem. Phys.* 79:2042–2053.

Alben, J. O., P. P. Moh, F. G. Fiamingo, and R. A. Altschuld. 1981. Cytochrome oxidase (a_3) heme and copper observed by low-temperature

Fourier transform infrared spectroscopy of the CO complex. *Proc. Nat. Acad. Sci. USA*. 78:234–237.

Alben, J. O., D. Beece, S. F. Bowne, W. Doster, L. Eisenstein, H. Frauenfelder, D., Good, J. D. McDonald, M. C. Marden, P. P. Moh, L. Reinisch, A. H. Reynolds, E. Shyamsunder, and K. T. Yue. 1982. Infrared spectroscopy of photodissociated carboxymyoglobin at low temperatures. *Proc. Natl. Acad. Sci. USA*. 79:3744–3748.

Ansari, A., J. Berendzen, S. F. Bowne, H. Frauenfelder, I. E. T. Iben, T. B. Sauke, E. Shyamsunder, and R. D., Young. 1985. Protein states and proteinquakes. *Proc. Natl. Acad. Sci. USA*. 82:5000–5004.

Ansari, A., J. Berendzen, D. Braunstein, B. R. Cowen, H. Frauenfelder, M. K. Hong, I. E. T. Iben, J. B. Johnson, P. Ormos, T. B. Sauke, R. Scholl, A. Schulte, P. J. Steinbach, J. Vittitow, and R. D. Young. 1987. Rebinding and relaxation in the heme pocket. *Biophys. Chem.* 26:337–355.

Antonini, E., and M. Brunori. 1971. Hemoglobin and myoglobin in their reactions with ligands. North-Holland, Amsterdam.

Austin, R. H., K. W. Beeson, L. Eisenstein, H. Frauenfelder, and I. C. Gunsalus. 1975. Dynamics of ligand binding to myoglobin. *Biochemistry*. 14:5355–5373.

Berendzen, J., and D. Braunstein. Temperature-derivative spectroscopy: a tool for protein dynamics. 1990. *Proc. Natl. Acad. Sci. USA*. 87:1–5.

Caughey, W. S., H. Shimada, M. G. Choc, and M. P. Tucker. 1981. Dynamic protein structures: infrared evidence for four discrete rapidly interconverting conformers at the carbon monoxide binding site of bovine heart myoglobin. *Proc. Natl. Acad. Sci. USA*. 78:2903–2907.

Dlott, D. D., H. Frauenfelder, P. Langer, H. Roder, and E. E. Di Iorio. 1983. Nanosecond flash photolysis study of carbon monoxide binding to the β chain of hemoglobin Zürich [β63(E7)His $\rightarrow$ Arg]. *Proc. Natl. Acad. Sci. USA*. 80:6239–6243.

Doster, W., D. Beece, S. F. Bowne, E. E. Di Iorio, L. Eisenstein, H. Frauenfelder, L. Reinisch, E. Shyamsunder, K. H. Winterhalter, and K. T. Yue. 1982. Control and pH dependence of ligand binding to heme proteins. *Biochemistry*. 21:4831–4839.

Ehrenstein D., and G. U. Nienhaus. 1992. Conformational substates in azurin. *Proc. Nat. Acad. Sci. USA*. 89:9681–9685.

Frauenfelder, H. 1978. Principles of ligand binding to heme proteins. *Methods Enzymol.* 54:506–532.

Frauenfelder, H., G. A. Petsko, and D. Tsernoglou. 1979. Temperature-dependent X-ray diffraction as a probe of protein structural dynamics. *Nature (Lond.)*. 280:558–563.

Frauenfelder, H. 1983. Dynamic aspects of protein reactions. *In* Structure and Dynamics: Nucleic Acids and Proteins. E. Clementi and R. H. Sarma, editors. Adenine Press, New York. 369–376.

Frauenfelder, H., F. Parak, and R. D. Young. 1988. Conformational substates in proteins. *Annu. Rev. Biophys. Biophys. Chem.* 17:451–479.

Frauenfelder, H., N. A. Alberding, A. Ansari, D. Braunstein, B. R. Cowen, M. K. Hong, I. E. T. Iben, J. B. Johnson, S. Luck, M. C. Marden, J. R. Mourant, P. Ormos, L. Reinisch, R. Scholl, A. Schulte, E. Shyamsunder, L. B. Sorensen, P. J. Steinbach, A.-H. Xie, R. D. Young, and K. T. Yue. 1990. Proteins and pressure. *J. Phys. Chem.* 94:1024–1037.

Frauenfelder, H., S. G. Sligar, and P. G. Wolynes. 1991. The energy landscapes and motions of proteins. *Science (Wash. DC)*. 254:1598–1603.

Fuchsman, W. H., and C. A. Appleby. 1979. CO and O_2 complexes of soybean leghemoglobins: pH effects upon infrared and visible spectra. Comparisons with CO and O_2 complexes of myoglobin and hemoglobin. *Biochemistry*. 18:1309–1321.

Hong, M. K., 1988. FTIR studies of the environmental effects on carbonmonoxy-myoglobin. Ph.D. thesis. University of Illinois at Urbana-Champaign. 117 pp.

Hong, M. K., D. Braunstein, B. R. Cowen, H. Frauenfelder, I. E. T. Iben, J. R. Mourant, P. Ormos, R. Scholl, A. Schulte, P. J. Steinbach, A. Xie, and R. D. Young. 1990. Conformational substates and motions in myoglobin. External influences on structure and dynamics. *Biophys. J.* 58: 429–436.

Iben, I. E. T., D. Braunstein, W. Doster, H. Frauenfelder, M. K. Hong, J. B. Johnson, S. Luck, P. Ormos, A. Schulte, P. J. Steinbach, A. H. Xie, and R. D. Young. 1989. Glassy behavior of a protein. *Phys. Rev. Lett.* 62: 1916–1919.

Kendrew, J. C., and R. G. Parish. 1956. The crystal structure of myoglobin. III. Sperm-whale myoglobin. *Proc. Roy. Soc. London. Ser. A*. 238:305–324.

Kuriyan, J., S. Wilz, M. Karplus, and G. A. Petsko. 1986. X-ray structure and refinement of carbon-monoxy (Fe II)-myoglobin at 1.5 Å resolution. *J. Mol. Biol.* 192:133–154.

Lavalette, D., and C. Tetreau. 1988. Viscosity-dependent energy barriers and equilibrium conformational fluctuations in oxygen recombination with hemerythrin. *Eur. J. Biochem.* 177:97–108.

Makinen, M. W., R. A. Houtchens, and W. S. Caughey. 1979. Structure of carboxymyoglobin in crystals and in solution. *Proc. Natl. Acad. Sci. USA*. 76:6042–6046.

McCoy, S., and W. S. Caughey. 1971. Infrared evidence for two types of bound CO in carbonyl myoglobins. *In* Probes of structure and function of macromolecules and membranes, probes of enzymes and hemoproteins. B. Chance, T. Yonetani, and A. Mildvan, editors. Vol. 2, 289–291.

Moore, J. N., P. A. Hansen, and R. M. Hochstrasser. 1988. Iron-carbonyl bond geometries of carboxymyoglobin in solution determined by picosecond time-resolved infrared spectroscopy. *Proc. Natl. Acad. Sci. USA*. 85:5062–5066.

Morikis, D., P. M. Champion, B. A. Springer, and S. G. Sligar. 1989. Resonance Raman investigations of site-directed mutants of myoglobin: effects of distal histidine replacement. *Biochemistry*. 28:4791–4800.

Nienhaus, G. U., J. R. Mourant, and H. Frauenfelder. 1992. Spectroscopic evidence for conformational relaxation in myoglobin. *Proc. Natl. Acad. Sci. USA*. 89:2902–2906.

Oldfield, E., K. Guo, J. D. Augspurger, and C. E. Dykstra. 1991. A molecular model for the major conformational substates in heme proteins. *J. Am. Chem. Soc.* 113:7537–7541.

Ormos, P., D. Braunstein, H. Frauenfelder, M. K. Hong, S. Lin, T. B. Sauke, and R. D. Young. 1988. Orientation of carbon monoxide and structure-function relationship on carbonmonoxy myoglobin. *Proc. Natl. Acad. Sci. USA*. 85:8492–8496.

Petrich, J. W., J.-C. Lambry, K. Kuczera, M. Karplus C. Poyart, and J.-L. Martin. 1991. Ligand binding and protein relaxation in heme proteins: a room temperature analysis of NO geminate recombination. *Biochemistry*. 30:3975–3987.

Quillin, M. L., R. E. Brantley Jr., K. A. Johnson, and G. N. Phillips. 1992. Kinetic and structural analysis of the effects of pH on carbon monoxide association in myoglobin. *Biophys J.* 61:466*a*. (Abstr.)

Shimada, H., and W. S. Caughey. 1982. Dynamic protein structures: effects of pH on conformer stabilities at the ligand-binding site of bovine heart myoglobin carbonyl. *J. Biol. Chem.* 257:11893–11900.

Steinbach, P. J., A. Ansari, J. Berendzen, D. Braunstein, K. Chu, B. R. Cowen, D. Ehrenstein, H. Frauenfelder, J. B. Johnson, D. C. Lamb, S. Luck, J. R. Mourant, G. U. Nienhaus, P. Ormos, R. Philipp, A. Xie, and R. D. Young. 1991. Ligand binding to heme proteins: connection between dynamics and function. *Biochemistry*. 30:3988–4001.

Straub, J. E., and M. Karplus. 1991. Molecular dynamics study of the photodissociation of carbon monoxide from myoglobin: ligand dynamics in the first 10ps. *Chem. Phys.* 158:221–248.

Stryer, L. 1988. Biochemistry. W. H. Freeman, San Francisco. 3rd Ed., 1089 pp.

Young, R. D., H. Frauenfelder, J. B. Johnson, D. C. Lamb, G. U. Nienhaus, R. Philipp, and R. Scholl. 1991. Time- and temperature dependence of large-scale conformational transitions in myoglobin. *Chem. Phys.* 158: 315–328.

Zhu, L., J. T. Sage, A. A. Rigos, D. Morikis, and P. M. Champion. 1992. Conformational interconversion in protein crystals. *J. Mol. Biol.* 224: 207–215.